First-principles study of γ-Al_2O_3 (100) surface

C. Y. Ouyang,[1,2,*] Ž. Šljivančanin,[2] and A. Baldereschi[2]
[1]*Department of Physics, Jiangxi Normal University, Nanchang 330022, China*
[2]*Institut Romand de Recherche Numérique en Physique des Matériaux (IRRMA), École Polytechnique Fédérale de Lausanne (EPFL), CH-1015 Lausanne, Switzerland*

(Received 13 January 2009; revised manuscript received 25 April 2009; published 11 June 2009)

The atomic and electronic structures of the γ-Al_2O_3 (001) surface are studied using the density-functional theory approach. From calculated surface energies for different surface terminations, we identified a mixed dense Al-O (001) layer, containing both octahedral aluminum and oxygen atoms, as the most stable γ-Al_2O_3 (001) surface. We found that environmental O_2 gas does not affect the surface stoichiometry. Comparison of the electronic structure of the surface and the bulk γ-Al_2O_3 shows that the band gap at the surface is slightly smaller than that of the bulk γ alumina due to the contributions of the surface O $2p$ states.

DOI: 10.1103/PhysRevB.79.235410 PACS number(s): 68.35.Md, 73.20.At, 82.65.+r, 81.05.Je

I. INTRODUCTION

Due to their high electronic resistance, good abrasion and corrosion resistance, high surface area, mechanical strength, and hardness, aluminum oxides are widely used in electronics, catalysis, surface coating, and thin-film devices.[1–3] Among the various metastable structures of Al_2O_3, the γ alumina (γ-Al_2O_3) is particularly important in the petroleum industry because of its applications as both an active catalyst[4] and a catalytic support.[5]

The wide technological applications of γ-Al_2O_3 have motivated many studies devoted to its basic physical properties, i.e., the crystal structure, distribution of the Al vacancies, and the electronic structure. The structure of γ-Al_2O_3 can exhibit either a spinel-like structure or nonspinel structure, depending on the way it is prepared.[6–11] γ-Al_2O_3 is derived from the thermal dehydration of boehmite. When the dehydration process is complete, there leaves no hydrogen in the γ-Al_2O_3 lattice. On the contrary, certain hydrogen may exist in the bulk structure. This makes the structure of γ-Al_2O_3 very complex. In a spinel-like γ-Al_2O_3, Al atoms are located at both the 8a positions (tetrahedrally coordinated by oxygen, denoted as T_d sites) and the 16d positions (octahedrally coordinated by oxygen, denoted as O_h sites). In order to satisfy the stoichiometry of γ-Al_2O_3, the spinel structure must contain $2\frac{2}{3}$ Al vacancies in average per spinel unit cell. Many experimental and theoretical investigations have been devoted to resolve the "old controversy" of whether the vacancies are located at the T_d sites or the O_h sites. Some studies show that the vacancies preferentially locate at O_h sites,[12,13] while other studies support that the vacancies are located at T_d sites[14,15] or even both T_d and O_h sites.[16] Most of the recent *ab initio* calculations tend to support that the vacancies are located at O_h sites[17,18] when hydrogen in the structure is not considered. Johansson *et al.* applied first-principles calculations to study the structure of the γ-Al_2O_3 and concluded that the vacancies are located at O_h sites. Yet, the energy differences they calculated between structures with all vacancies located on O_h sites and structures with some (or all) vacancies located at T_d sites are quite small. This might be due to the rather small unit cell they used, which does not allow even distribution of the vacancies. More recently, the old controversy is resolved, and it is clear that the vacancy distribution in γ-Al_2O_3 is sensitive to the existence of hydrogen in the structure.[19,20] Without hydrogen in the lattice, vacancies in O_h sites are energetically favorable than in T_d sites, and widely separated vacancies are energetically favorable than near-neighboring vacancies. However, upon incorporation of hydrogen into the structure, "clusters" of near-neighbor vacancies are slightly energetically preferred.[19]

The surface properties of γ-Al_2O_3 have also attracted considerable interest. Vijay *et al.*[21] studied the vacancy distribution near the γ-Al_2O_3 (001) surface. They found that the vacancies prefer to be in the bulk rather than at the surface. Pinto *et al.*[22] performed *ab initio* calculations to investigate various surfaces of γ-Al_2O_3. They compared in detail the surface relaxation and surface energies among various surfaces of γ-Al_2O_3 and α-Al_2O_3 (0001) basal plane. γ-Al_2O_3 can be used as a catalyst,[1,4] and thus the surface reactivity of γ-Al_2O_3 is studied extensively. For example, surface reconstruction and surface Lewis acidity of γ-Al_2O_3 are studied by Sohlberg *et al.*[23] However, to our best knowledge, detailed information on the surface electronic structure of the γ-Al_2O_3 surfaces available in the literature is limited, which is certainly very important to the surface related applications.

In the present work, we apply *ab initio* calculations to investigate structural and electronic properties of the γ-Al_2O_3 (001) surface in order to propose a realistic model for the surface in vacuum or exposed to an oxygen atmosphere. The paper is organized as follows: after presenting the computational methods applied throughout this study, we describe the bulk model of the γ-Al_2O_3 and give an account of the results to its atomic and electronic structures. Then, we focus on the structural and electronic properties of the γ-Al_2O_3 (001) surface, describe different structural models considered in the present study, and identify the one with the lowest total energy. The effect of the O_2 environment on the surface structure is also investigated. At last, we conclude the paper with a summary of the main results.

II. COMPUTATIONAL DETAILS

Calculations in the present study are performed using the DACAPO code,[24] employing ultrasoft pseudopotentials.[25,26]

The valence electron wave functions and the augmented electron density are expanded in the plane-wave basis sets with cutoff energies of 25 and 40 Ry, respectively. The Perdew-Wang exchange-correlation functional (PW91) (Ref. 27) is used to describe electronic exchange-correlation effects. The theoretically determined lattice constant of 7.958 Å is used throughout the present study. Atomic positions are relaxed until the second norm of the forces acting on all relaxed atoms is less than 0.05 eV/Å. In order to satisfy the Al_2O_3 stoichiometry, a large $1\times1\times3$ supercell, containing 160 atoms, and the $3\times3\times1$ Monkhorst-Pack[28] scheme **k**-point sampling are used to calculate bulk properties of the γ-Al_2O_3. For all the surface calculations, slabs with 24 (or 25) atomic layers are used, with vacuum thickness of ~12 Å, in order to avoid the interaction due to the periodic boundary conditions. The convergence of the total energy with respect to the **k**-point sampling has been carefully examined. The electrostatic field within vacuum is very weak and the dipole corrections are not included except for testing purposes.

III. RESULTS AND DISCUSSIONS

A. Bulk model and electronic structure

In the present study, to make problems simpler, hydrogen in the bulk is not considered. We adopt the spinel structure of γ-Al_2O_3, with the space group $Fd\bar{3}m$.[29] Within one spinel γ-Al_2O_3 unit cell, there are 32 oxygen atoms, occupying 32*e* Wyckoff positions, packed in the fcc arrangement. Al atoms are located at both the 8*a* (T_d sites) and the 16*d* (O_h sites) positions. The cation to anion ratio is 3:4 in an ideal spinel structure, which is significantly different from the 2:3 ratio in the γ-Al_2O_3. In order to satisfy the stoichiometry of the γ-Al_2O_3, it contains $2\frac{2}{3}$ Al vacancies per spinel unit cell in average. Thus, a supercell containing three unit cells (160 atoms and 8 Al vacancies) is required to satisfy both the Al_2O_3 stoichiometry and the vacancy distribution requirements. However, it is difficult to try all vacancy distribution possibilities with such a large supercell. Due to limited computational power, in most of the previous theoretical investigations, relatively small unit cells were used. In these models, the stoichiometry was different from the real case and the distances between the Al vacancies were sometimes too small.

In order to obtain a good bulk model, the following two assumptions have been taken into account: (1) the vacant spinel sites are preferred to take octahedral positions and (2) the vacant spinel sites want to be located as far as possible from each other and thus distribute as evenly as possible in the lattice. These assumptions are generally accepted by other studies.[18,21] In the present study, a single cubic unit cell (Al_2O_3 stoichiometry is not satisfied with this unit cell) was used to test the above two assumptions. Within the unit cell all vacancy distribution possibilities are considered and tested. The results support these two assumptions as expected. However, the calculated electronic structure does not satisfy the intrinsic insulating characteristics of Al_2O_3. Figure 1(a) is the total density of states (DOS) of the energetically most favorable configuration (denoted as B1 in the following). This unreasonable electronic structure could be ascribed to the broken stoichiometry. There are 22 Al atoms and 32 O atoms within the B1 unit cell; if each Al atom donates three electrons and each O atom accepts two electrons, there will be two excess electrons in the system. From Fig. 1(a), it seems that these two electrons lie in the middle of the gap and thus move up the Fermi level. To verify this point, we removed two electrons from the system (through the program) and the insulating characteristics appear, as shown in Fig. 1(b). However, removing electrons from the system is not physically realistic. The only physical way to solve this problem is to construct a large supercell, which can satisfy the stoichiometry of Al_2O_3 and the vacancy distribution requirements at the same time.

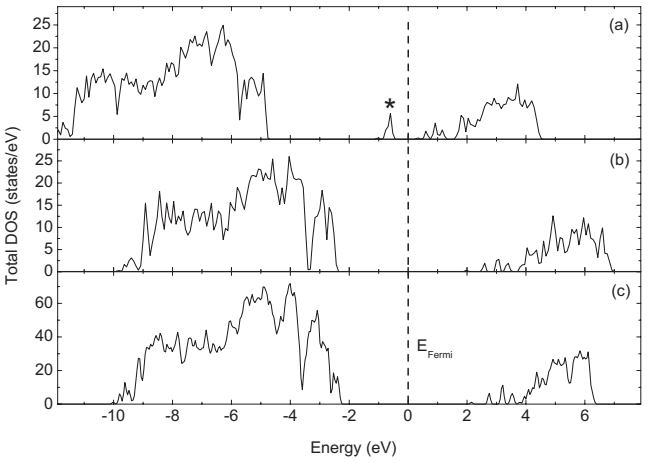

FIG. 1. Total density of states of bulk γ-Al_2O_3 calculated with (a) B1 configuration, (b) B1 configuration after removing two electrons from the system, and (c) the optimized $1\times1\times3$ supercell. The Fermi level is aligned to 0 and a Gaussian broadening width of 0.05 eV was used.

Following the above two assumptions, four different vacancy distribution models are considered within a $1\times1\times3$ supercell. The atomic positions are fully optimized for each configuration and the one with the lowest total energy is shown in Fig. 2 and chosen as the bulk model in the present work. The calculated lattice constant is 7.958 Å, which is slightly larger than the experimental value of 7.911 Å,[29,30] but within the scope of reasonable error of the generalized gradient approximation (GGA) calculations. The predicted bulk modulus is 199.7 GPa, which is also in good agreement with experimental value and other GGA-based theoretical results.[18,22] Figure 1(c) shows the total DOS calculated within the supercell. The shape of the DOS and width of the valence band agree well with the experimental results.[12] Our calculations confirm highly insulating properties of the γ-Al_2O_3, with a band gap of about 4.4 eV. Similar values for the energy gap have been reported in other theoretical works for both spinel based models[13,18] and nonspinel models.[7,31] However, these values are much smaller than experimental value of ~8.7 eV (Ref. 12) due to the well-known intrinsic shortcoming of density-functional theory (DFT)-based calculations.[32]

From analysis of the DOS projected on atomic orbitals we find out that the valence band is mainly originated from the

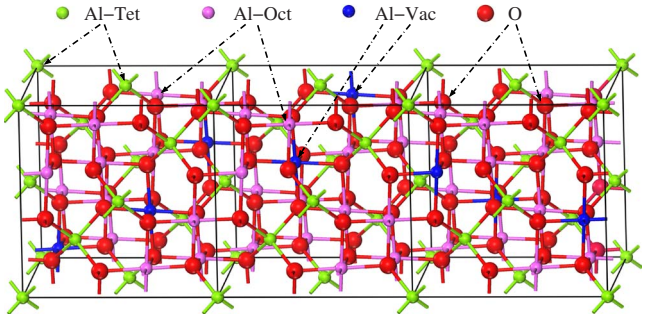

FIG. 2. (Color online) The energetically most favorable configuration of the $1\times1\times3$ supercell. The red (large, marked with "O") atoms are O, the green (small, marked with "Al-Tet") atoms are tetrahedral site Al, the purple (small, marked with "Al-Oct") atoms are octahedral site Al, and the blue (small, marked with "Al-Vac") ones are the vacant octahedral sites.

O $2p$ states, while the conduction band is formed by both Al $2s$, Al $2p$ states and the O $2p$ states. The fact that the Al states contribute to the conduction band indicates that the Al-O bond in γ-Al_2O_3 is not purely ionic, and the Al-O covalent character cannot be neglected.

B. γ-Al_2O_3 (001) surface

Starting from the optimized structure of the bulk γ-Al_2O_3, as described in Sec. III A, and using the slab approach, we constructed several different models of the γ-Al_2O_3 (001) surface. We first address the issue of stoichiometry at the surface, as it has profound effect on the electronic structure of the γ-Al_2O_3 (001) surface. The structure of the bulk γ-Al_2O_3 can be viewed as an alternating stacking sequence of the low-density and high-density layers along the [001] direction. The former contain only tetrahedral Al atoms, while the later are composed of both O atoms and octahedral Al atoms, in addition to some possible Al vacancies (see Fig. 2). Therefore, there are two possible terminations for the γ-Al_2O_3 (001) surface: one with only tetrahedral Al atoms in the surface layer (low-density layer) and the other with mixed octahedral Al atoms and O atoms in the surface (high-density layer). As the bulk γ-Al_2O_3 is stacked alternatively with low-density and high-density layers along the [001] direction, when we cleave the (001) surface directly from bulk, a low-density surface and a high-density surface are created at opposite sides of the slab. Thus, to create a surface model with only one type of the surface we applied the following procedure.

We assume that when we cleave the surface along the low-density plane (only two Al atoms in the slab model), the plane itself is broken down, one Al atom from the broken plane is adsorbed on one side of the slab and the other Al atom is adsorbed at the equivalent site on the opposite side of the slab. The slab terminates with two identical surfaces, while the bulk stoichiometry of the γ-Al_2O_3 is preserved. For Al atoms from the broken low-density layer we considered three possible dispositions: (i) the Al atoms keep their initial positions from bulk (or equivalent positions on the opposite side of the slab), forming high-density layer terminated surfaces with Al adatoms on them. We denote this configuration as S1. However, upon the structure optimization the S1 configuration will encounter large relaxations, and finally we find out that the Al atoms will drop down to the high-density layers. (ii) At both sides of the slab, one Al atom from each of the subsurface high-density layers migrates to the surface and forms a slab terminated by low-density layers (denoted as S2). However, in the bulk model, the vacant sites are distributed as evenly as possible, and at least one of the high-density subsurface layers must contain one Al vacant site. Therefore, in the S2 configuration, there are two vacant sites in one high-density plane. Obviously, this is not energetically favorable as the vacancies prefer to locate as far as possible from each other. (iii) If the bulk sample is cleaved along the low-density layer with two vacant sites (one at each side) at the two neighboring high-density planes, then Al atoms from the broken down low-density layer could diffuse and fill into those vacant sites at the high-density layers and form the slab terminated with high-density layers, denoted as the S3 (see Fig. 3).

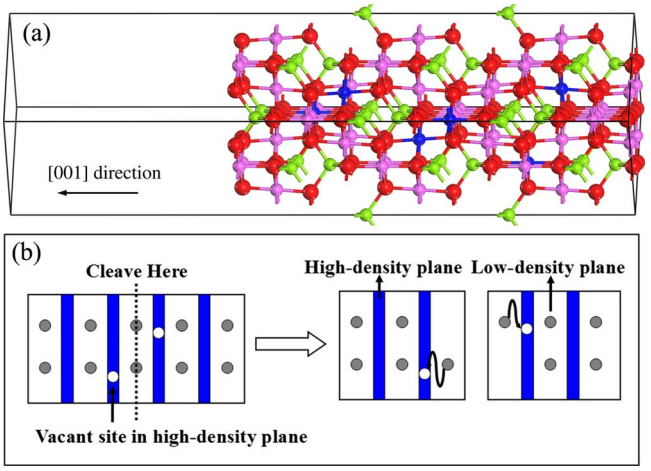

FIG. 3. (Color online) (a) The slab model of S3 configuration of γ-Al_2O_3 (001) surface and (b) the schematical picture of cleaving surfaces along the low-density plane. The size and color of atoms are the same as in Fig. 2.

The calculated results show that configuration S3 is the one with the lowest total energy. Table I gives the surface energies for all configurations we considered. From Table I, it can be seen that surface energies of S1 and S3 configurations are much lower than those of the other configurations. This shows that the high-density terminated surfaces are more stable than the low-density terminated ones. Furthermore, the surface energy of the S3 configuration is lower than that of the S1 configuration, which implies that the vacancies are located in the bulk rather than on the surface, in agreement with previous studies.[21] In Table I we also list the surface energy of the α-(0001) Al-terminated surface, which is the most stable α-alumina surface.[33] The calculated surface energy of the α-Al_2O_3 (0001) is 2.536 J/m^2, which is much higher than that of the S3 configuration. The fact that the γ-Al_2O_3 has lower surface energy but higher bulk energy implies that the γ-Al_2O_3 could be thermodynamically more stable when the molar surface area is higher than a critical point. In the present study, the calculated bulk-energy differ-

TABLE I. Calculated surface energy for different terminations of γ-Al_2O_3 (001) surfaces.

Configurations	Surface energy (J/m^2)		
	Slab size (atoms)	Before relaxation	After relaxation
S1	160	3.154	1.371
S2	160	4.394	3.473
S3	160	2.130	0.899
S4[a]	162	2.204	1.705
Ref. 22	100	2.97	1.05
α (0001)[b]	60	3.547	2.536

[a]S4 is low-density terminated surface (without right Al_2O_3 stoichiometry). When we cut the bulk directly, the slab has one low-density plane on one side and one high-density plane on the other side. Then S4 is constructed by adding one low-density layer at the top of the high-density plane. As it has different atom number from the bulk, the surface energy here has taken bulk metal Al as reference.

[b]α-Al_2O_3 Al-terminated (0001) surface, calculated with the same pseudopotential.

ence between the α and the γ-Al_2O_3 is 0.254 eV/f.u. while the calculated surface energy difference is 1.637 J/m^2. With these values, we evaluated the critical point to be about 147 m^2/g, which is consistent with the experimental findings.[34] More interestingly, we also estimated the critical ultrathin film thickness for γ-Al_2O_3 of ~36 Å (with both surfaces exposed to vacuum). Above this thickness, the γ-Al_2O_3 phase would be thermodynamically unstable.

As mentioned above, the S3 configuration is constructed through filling into the vacant sites on the surface with the Al atoms from the broken down low-density layer. The S3 configuration is the thermodynamically most favorable model of the γ-Al_2O_3 (001) among configurations considered here. However, vacancy diffusion in the bulk γ-Al_2O_3 or diffusion from the surface to the bulk is accompanied with an activation energy in range from 1 to 3 eV.[21] Hence, the vacancy distribution is mainly frozen at room temperature. If the activation energy for migration of the Al atom from the surface low-density layer into the vacant site in the high-density subsurface is comparable to the energy barrier of the vacancy diffusion in the bulk, then the S3 configuration, although thermodynamically favorable, would not be kinetically accessible at room temperature. However, the diffusion pathway that occurs on a surface is usually different from that in the bulk. Using the nudged elastic band (NEB) method[35,36] we calculated the diffusion pathway for one Al atom migrating into the subsurface vacant site in the high-density layer. As the migration process occurs on the surface and the NEB calculations are quite computationally expensive, it is not necessary to use the same large slab (24 layers and 160 atoms) as it is done for the total-energy and electronic-structure calculations. Here since only six top layers of the slab are relaxed in the calculations, the NEB calculation can be done by taking only these six top layers into account. At the same time, to save computational costs, only the Γ point is used for the NEB calculation.

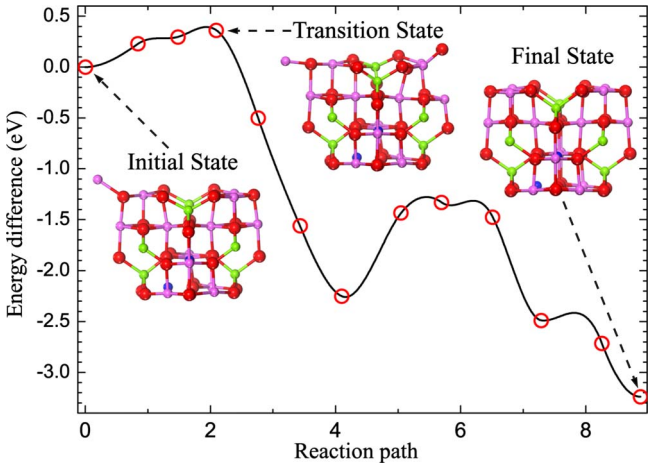

FIG. 4. (Color online) Energy barrier for one Al atom filling into the vacant site on the surface. The images start from the relaxed structure of the surface and end at the final position. The cycles are the energy differences to the starting image for each image along the reaction path. The insets are the initial, transition, and final states viewing from the [110] direction of the lattice. The color and size of atoms and vacancies are the same as in Fig. 2

Figure 4 shows changes in the total energy along the optimized reaction path. The energy barrier for migrating the Al atom into the vacant site on the surface is 0.36 eV, which is much lower than that of the Al vacancy diffusion in the bulk. With such a small energy barrier, the migration process can quickly occur at room temperature.

The insets of Fig. 4 show the initial and final states, together with the transition state along an optimized diffusion pathway obtained from the NEB calculation. From the insets of Fig. 4, we can see that the initial state corresponds to the bulk position of the migrating Al atom. In the final state, the migrating Al atom occupies the former vacant site in the high-density layer. The transition state corresponding to the migrating Al atom comes down to the surface plane and locates between two O atoms. At the same time, one of these two O atoms in between is pushed by the migrating Al atom and lifted up a little. The relaxation of the O atom lowers the total energy of the transition state to some extent and in turn the energy barrier of the migration process.

C. Surface thermodynamics

From the above discussions, we conclude that under vacuum conditions, the S3 is the most stable among investigated configurations of the γ-Al_2O_3 (001) surface. In reality the interactions between the surface and the surrounding environment should be taken into account. In the case of the α-Al_2O_3 (0001) surface, the surface structural stability is strongly dependent on the surface environments. For example, the O-terminated α-Al_2O_3 (0001) surface is not stable in the vacuum but becomes stable when H atoms are present on the surface.[37,38] In the case of the γ-Al_2O_3, the situation is even more complicated. Both the H and the O (or the OH group and water) could play an important role to the surface morphology and stability and thus are important to the catalysis, adhesion, and corrosion properties.[39]

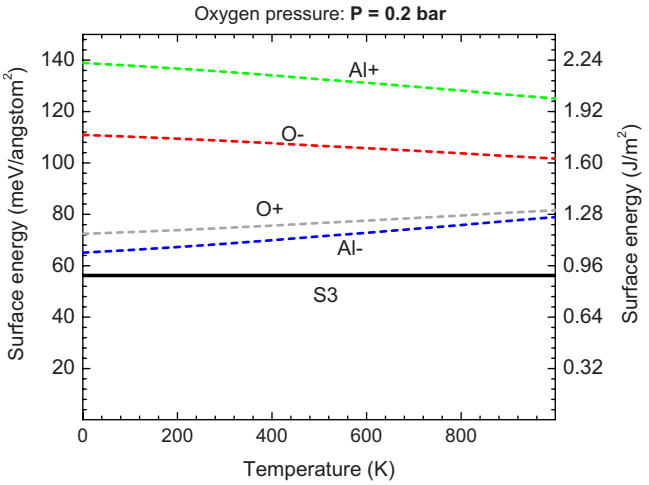

FIG. 5. (Color online) Surface free energy of different γ-Al_2O_3 (001) surfaces as a function of temperature at given oxygen-partial pressure $P=0.2$ bar.

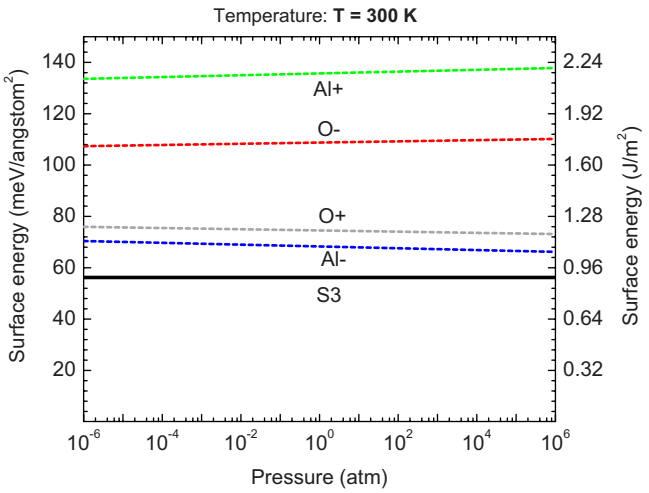

FIG. 6. (Color online) Surface free energy of different γ-Al_2O_3 (001) surfaces as a function of oxygen-partial pressure at a room temperature $T=300$ K.

In the present study, we focus on the influence of the oxygen environment on the γ-Al_2O_3 (001) surface stability. Namely, we consider a system with a large gas-phase region consisting of molecular oxygen at certain pressure and the γ-Al_2O_3 surface in contact with the gas-phase oxygen. When the system is in thermodynamical equilibrium, we assume that the oxygen chemical potential is equal in the gas-phase region and at the surface, and the Al chemical potential at the surface is the same as in the bulk. The chemical potential of the gas-phase oxygen molecules at $T=0$ and $P=0$, denoted as the $\mu_O(T_0,P_0)$, is extracted from DFT calculations. The temperature-dependence contribution to the oxygen chemical potential at given pressure P_1, denoted as the $\mu_O(T_0,P_1)$, is taken from experiment.[40] For simplicity, to estimate the pressure-dependence contribution to the oxygen chemical potential, the gas-phase oxygen is treated as an ideal gas. With these assumptions, the oxygen chemical potential can be written as

$$\mu_O(T,P) = \mu_O(T_0,P_0) + \mu_O(T,P_1) + \frac{1}{2}k_B T \ln\left(\frac{P}{P_1}\right). \quad (1)$$

We take the oxygen chemical potential as the only independent variable in the system, while the chemical potential for 1 f.u. of the γ-Al_2O_3 is taken from the bulk calculation. The Gibbs free energy of the surface at temperature T and oxygen partial pressure P is written as[37,41]

$$G(T,P) = E_{slab} - \frac{1}{2}N_{Al}\mu^{bulk}_{Al_2O_3} + \left(\frac{3}{2}N_{Al} - N_O\right)\mu_O(T,P). \quad (2)$$

In the present study, Eq. (2) is used to investigate the influence of the oxygen environment on the stoichiometry of the γ-Al_2O_3 (001) surface. Starting from the S3 surface configuration, different surface models with different stoichiometries were considered. We constructed four nonstoichiometrical models by adding or removing one Al or one O atom from the S3 configuration. Newly created configurations are denoted as the Al+, Al–, O+, and O–, respectively. Figure 5 presents calculated free energies of the S3 and four nonstoichiometric surfaces as a function of temperature at a constant oxygen partial pressure of 0.2 bar, which is close to oxygen partial pressure in the atmosphere. The figure shows that in the temperature range from 0 to 1000 K, the S3 configuration is thermodynamically more stable than any of nonstoichiometric models.

Similarly, at room temperature ($T=300$ K), the surface free energy of all nonstoichiometry surfaces as a function of oxygen partial pressure is shown in Fig. 6. In this case, the S3 configuration is also thermodynamically more stable than the nonstoichiometric surfaces over a very large pressure range. Thus, it can be concluded that the S3 configuration is more stable than the nonstoichiometric configurations at all experimentally reasonable temperatures and oxygen partial pressures, indicating that the oxygen atmosphere does not affect the chemical composition of the γ-Al_2O_3 (001) surface created in the vacuum.

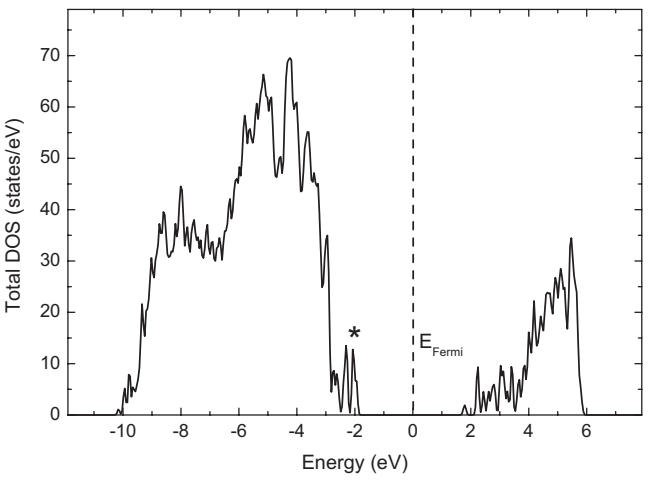

FIG. 7. Total density of states of the S3 γ-Al_2O_3 (001) surface. The Fermi level is aligned to 0 and a Gaussian broadening width of 0.05 eV was used.

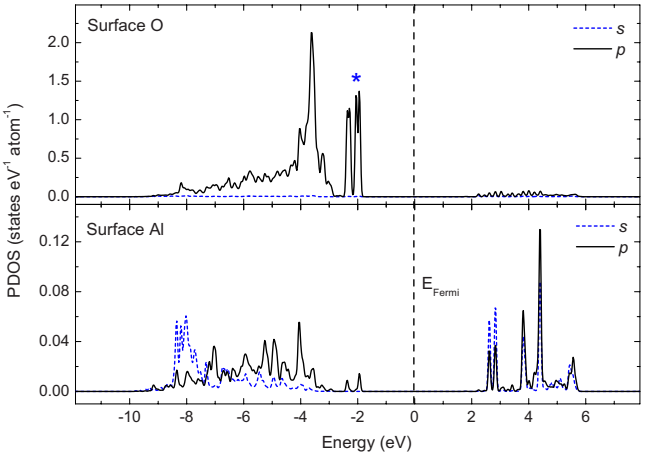

FIG. 8. (Color online) Atomic-projected DOS on O and Al atoms at the γ-Al_2O_3 (001) surface of S3 configuration. Solid and dashed lines for p and s states, respectively. Note the different scales in the plots.

D. Surface electronic structures

Shown in Fig. 7 is the total DOS of the γ-Al_2O_3 (001) S3 surface. As in the bulk, the (001) surface of γ-Al_2O_3 exhibits insulating properties, with a band gap of about 3.5 eV, smaller by 0.9 eV than the bulk. This reduction in the band-gap size is mainly due to the states at the top of the valence band (marked by a star in Fig. 7). Those states do not appear in the DOS of bulk γ-Al_2O_3 (see Fig. 1). To clarify the character of these states we calculated DOS projected on the atomic orbitals. The atom projected DOSs for the Al and O atoms from the surface and inside of the slab are shown in Fig. 8. Figure 8(a) clearly shows that the states at the top of the valence band are mainly the $2p$ states of the surface O atoms. This is further verified by plotting the wave function of the highest occupied electronic state at the Γ point. Figure 9 shows that the wave function is dumbbell shaped, and the center of each dumbbell is on a surface O atom. This confirms the O $2p$ character of the surface states. The reasons why the surface O $2p$ states are positioned at higher energies than the corresponding bulk states are complex and probably include the surface relaxation and different electrostatic interactions present at the surface compared to the bulk.

IV. SUMMARY

In summary, the stability and surface electronic structure of γ-Al_2O_3 (001) surfaces are studied in detail from *ab initio* calculations. In order to satisfy the Al_2O_3 stoichiometry and the Al vacancy distribution requirements, large supercell bulk models are used in the present study. With this large bulk model, different (001) surface models are constructed and the calculated surface energies show that the S3 configuration is the most stable one. Then, the migration pathway of one Al atom diffusing on the surface to fill a vacant site is calculated with the NEB method, and the diffusion energy barrier is calculated to be about 0.36 eV, which shows that S3 can be formed even under room temperature. Furthermore, the surface thermodynamic studies show that the stoichiometric S3 configuration is more stable than other nonstoichiometric surfaces under a very large range of temperature and oxygen partial pressure conditions. The electronic structure of the S3 configuration surface model is studied and compared with the bulk in detail, results show that both the bulk and the surface exhibit insulating properties, and the band gap of the surface is a little smaller than the bulk. The atomic projected DOS and the wave-function plots show that the surface oxygen $2p$ states are the main reason for the lowered band gap of the surface. Furthermore, the atomic projected DOS also shows that Al atoms have some contributions to the conduction band for both bulk and surface cases, indicating that γ-Al_2O_3 is not purely an ionic oxide and the Al-O covalence effect cannot be neglected.

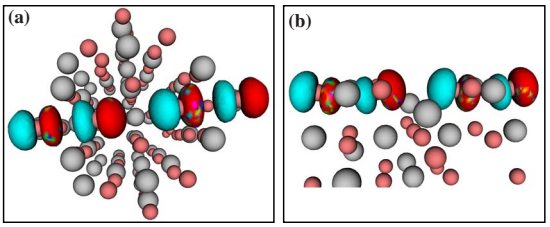

FIG. 9. (Color online) (a) Top view and (b) side view of the wave functions corresponding to the states at the top of the valence band marked by stars in Fig. 7. The gray (middle sized) and red (small sized) spheres are Al and O atoms, respectively; the large dumbbell is the shape of the wave function. For each dumbbell, different colors at each side represent different phases of the wave function.

ACKNOWLEDGMENTS

The calculations were performed at the central computational facilities of the École Polytechnique Fédérale de Lausanne and at the Swiss Center for Scientific Computing. This work was partly supported by the Swiss National Science Foundation under Grant No. 200020-112318.

*chuying.ouyang@epfl.ch

[1] G. Ertl, H. Knozinger, and J. Weitkamp, *The Handbook of Heterogeneous Catalysis* (Wiley, Weinheim, 1997).
[2] S. Wang, A. Y. Borisevich, S. N. Rashkeev, M. V. Glazoff, K. Sohlberg, S. J. Pennycook, and S. Pantelides, Nature Mater. **3**, 143 (2004).
[3] L. J. Liu, L. Q. Chen, X. J. Huang, X. Q. Yang, W. S. Yoon, H. S. Lee, and J. McBreen, J. Electrochem. Soc. **151**, A1344 (2004).
[4] H. Knozinger and P. Ratnasamy, Catal. Rev. - Sci. Eng. **17**, 31 (1978).
[5] B. C. Gates, J. R. Katzer, and G. A. Schuit, *Chemistry of Catalytic Processes* (McGraw-Hill, New York, 1979).
[6] G. Paglia, C. E. Buckley, A. L. Rohl, B. A. Hunter, R. D. Hart, J. V. Hanna, and L. T. Byrne, Phys. Rev. B **68**, 144110 (2003).
[7] E. Menendez-Proupin and G. Gutiérrez, Phys. Rev. B **72**,

035116 (2005).
[8] M. Sun, A. E. Nelson, and J. Adjaye, J. Phys. Chem. B **110**, 2301 (2006).
[9] M. Digne, P. Raybaud, P. Sautet, B. Rebours, and H. Toulhoat, J. Phys. Chem. B **110**, 20719 (2006).
[10] G. Paglia, C. E. Buckley, and A. L. Rohl, J. Phys. Chem. B **110**, 20721 (2006).
[11] A. Nelson, M. Sun, and J. Adjaye, J. Phys. Chem. B **110**, 20724 (2006).
[12] B. Ealet, M. H. Elyakhloufi, E. Gillet, and M. Ricci, Thin Solid Films **250**, 92 (1994).
[13] S. D. Mo, Y. N. Xu, and W. Y. Ching, J. Am. Ceram. Soc. **80**, 1193 (1997).
[14] R. Dupree, M. H. Lewis, and M. E. Smith, Philos. Mag. A **53**, L17 (1986).
[15] V. Jayaram and C. G. Levi, Acta Metall. **37**, 569 (1989).
[16] M. H. Lee, C. F. Cheng, V. Heine, and J. Klinowski, Chem. Phys. Lett. **265**, 673 (1997).
[17] F. H. Streitz and J. W. Mintmire, Phys. Rev. B **60**, 773 (1999).
[18] G. Gutiérrez, A. Taga, and B. Johansson, Phys. Rev. B **65**, 012101 (2001).
[19] C. Wolverton and K. C. Hass, Phys. Rev. B **63**, 024102 (2000).
[20] K. Sohlberg, S. J. Pennycook, and S. T. Pantelides, J. Am. Chem. Soc. **121**, 7493 (1999).
[21] A. Vijay, G. Mills, and H. Metiu, J. Chem. Phys. **117**, 4509 (2002).
[22] H. P. Pinto, R. M. Nieminen, and S. D. Elliott, Phys. Rev. B **70**, 125402 (2004).
[23] K. Sohlberg, S. J. Pennycook, and S. T. Pantelides, J. Am. Chem. Soc. **123**, 26 (2001).
[24] B. Hammer, L. B. Hansen, and J. K. Nørskov, Phys. Rev. B **59**, 7413 (1999).
[25] D. Vanderbilt, Phys. Rev. B **41**, 7892 (1990).
[26] K. Laasonen, A. Pasquarello, R. Car, C. Lee, and D. Vanderbilt, Phys. Rev. B **47**, 10142 (1993).
[27] J. P. Perdew, J. A. Chevary, S. H. Vosko, K. A. Jackson, M. R. Pederson, D. J. Singh, and C. Fiolhais, Phys. Rev. B **46**, 6671 (1992).
[28] H. J. Monkhorst and J. D. Pack, Phys. Rev. B **13**, 5188 (1976).
[29] R. S. Zhou and R. L. Snyder, Acta Crystallogr., Sect. B: Struct. Sci. **47**, 617 (1991).
[30] Y. G. Wang, P. M. Bronsveld, J. Th. M. DeHosson, B. Djuricic, D. McGarry, and S. Pickering, J. Am. Ceram. Soc. **81**, 1655 (1998).
[31] M. Digne, P. Sautet, P. Raybaud, P. Euzen, and H. Toulhoat, J. Catal. **226**, 54 (2004).
[32] V. Fiorentini and A. Baldereschi, Phys. Rev. B **51**, 17196 (1995).
[33] R. Di Felice and J. E. Northrup, Phys. Rev. B **60**, R16287 (1999).
[34] J. M. McHale, A. Auroux, A. J. Perrotta, and A. Navrotske, Science **277**, 788 (1997).
[35] G. Henkelman and H. Jonsson, J. Chem. Phys. **113**, 9978 (2000).
[36] G. Henkelman, B. P. Uberuaga, and H. Jonsson, J. Chem. Phys. **113**, 9901 (2000).
[37] X. G. Wang, A. Chaka, and M. Scheffler, Phys. Rev. Lett. **84**, 3650 (2000).
[38] A. Marmier and S. C. Parker, Phys. Rev. B **69**, 115409 (2004).
[39] S. N. Rashkeev, K. Sohlberg, S. P. Zhuo, and S. T. Pantelides, J. Phys. Chem. C **111**, 7175 (2007).
[40] D. R. Stull and H. Prophet, *JANAF Thermochemical Tables*, 2nd ed. (U. S. National Bureau of Standards, Washington, DC, 1971).
[41] W. Bergermayer, H. Schweiger, and E. Wimmer, Phys. Rev. B **69**, 195409 (2004).